Int. J. Heat Mass Transfer. Vol. 35, No. 4, pp. 913–925, 1992
Printed in Great Britain

0017-9310/92 $5.00 + 0.00
Pergamon Press plc

Local interfacial area measurement in bubbly flow

S. T. REVANKAR and M. ISHII†
School of Nuclear Engineering, Purdue University, West Lafayette, IN 47907, U.S.A.

(*Received* 7 *August* 1990 *and in final form* 20 *March* 1991)

Abstract—A theoretical foundation of the measurement method for the time averaged local interfacial area using a double sensor probe is presented. Experimental data are presented on the radial profiles of the void fraction, bubble velocity, bubble chord length and interfacial area concentration at various gas flow rates. In addition to these, some statistical information on turbulent motions of bubbles are presented. Each of the double sensors is checked against the global void measurement using a differential pressure. The result is very satisfactory. Furthermore, the area averaged void fraction and the interfacial area concentration obtained from the double sensor probe measurement compared very well with the photographic measurements. The results show that the double sensor probe method is accurate and reliable for the local measurements of interfacial area and void fraction in bubbly two-phase flow. Some results of the measurement of interfacial area concentration with the double sensor probe are also presented for bubbly flow at different liquid flow rates.

1. INTRODUCTION

IN THE analysis of two-phase flow thermal-hydraulics, various formulations such as the homogeneous flow model, drift flux model and two-fluid model have been proposed. Among these formulations, the two-fluid model [1, 2] considers each phase separately in terms of two sets of conservation equations which govern the balance of mass, momentum and energy of each phase. Because of its detailed treatment of the phase interactions at the interface, the two-fluid formulation can be considered the most accurate model. Since mass, momentum and energy are exchanged from one phase to the other through the interface, the interfacial transfer terms should be modeled accurately for the two fluid model to be useful. In the present state of the art, the constitutive equations for these interfacial terms are the weakest link in the two-fluid model. The difficulties arise due to the complicated transfer mechanisms at the interfaces affected by the motion and geometry of the interfaces. Furthermore, the constitutive equations should be modeled by macroscopic variables based on proper averaging. The importance of interfacial area concentration can be explicitly seen in the basic conservation equations of two-phase flow. For most applications, the model developed in ref. [1] can be written in the following forms:

continuity equation

$$\frac{\partial \alpha_k \rho_k}{\partial t} + \nabla \cdot (\alpha_k \rho_k \mathbf{v}_k) = \Gamma_k ; \quad (1)$$

momentum equation

$$\frac{\partial \alpha_k \rho_k \mathbf{v}_k}{\partial t} + \nabla \cdot (\alpha_k \rho_k \mathbf{v}_k \mathbf{v}_k) = -\alpha_k \nabla p_k + \nabla \cdot \alpha_k (\bar{\tau}_k + \tau_k^t) + \alpha_k \rho_k \mathbf{g} + \mathbf{v}_{ki} \Gamma_k + \mathbf{M}_{ik} - \nabla \alpha_k \cdot \tau_i ; \quad (2)$$

enthalpy energy equation

$$\frac{\partial \alpha_k \rho_k H_k}{\partial t} + \nabla \cdot (\alpha_k \rho_k H_k \mathbf{v}_k) = \nabla \cdot \alpha_k (\bar{q}_k + q_k^t) + \alpha_k \frac{D_k}{Dt} p_k + H_{ki} \Gamma_k + \frac{q''_{ki}}{L_s} + \Phi_k . \quad (3)$$

Here Γ_k, M_{ik}, τ_i, q''_{ki}, and Φ_k are the mass generation, the generalized interfacial drag, the interfacial shear stress, the interfacial heat flux, and the dissipation, respectively. The subscripts k and i denote phase k and the value at the interface, respectively. The α_k, ρ_k, $\mathbf{v}_k$, p_k and H_k denote the void fraction, the density, the velocity, the pressure, and the enthalpy of phase k. The $\bar{\tau}_k$, τ_k^t, $\bar{q}_k$, q_k^t and g denote the average viscous stress, the turbulent stress, the mean conduction heat flux, the turbulent heat flux, and the acceleration due to gravity. H_{ki} is the enthalpy of phase k at the interface. L_s is a length scale at the interface and $1/L_s$ has the physical meaning of the interfacial area per unit volume [1]. Then

$$\frac{1}{L_s} = a_i = \frac{\text{Interfacial area}}{\text{Mixture volume}} . \quad (4)$$

The interfacial transfer terms which appear on the right-hand side of equations (1)–(3) are related to each other through the averaged local jump conditions [1]. In order to develop constitutive relations for $\mathbf{M}_{ik}$, q''_{gi}/L_s and q''_{fi}/L_s, the knowledge of the interfacial area

† Author to whom correspondence should be addressed.

NOMENCLATURE

$\bar{a}_i^t$	time averaging of a_i
D_s	bubble surface mean diameter
D_v	bubble volume mean diameter
D_{vs}	Sauter mean diameter
j_g, j_f	superficial velocity of gas and liquid
N_t	number of bubbles or droplets passing a point per unit time
Δs	spacing between tip and rear sensor of double probe
t_j	time when jth interface passes the probe
$\mathbf{v}_{ij}$	velocity of jth interface
$\mathbf{v}_{izj}$	z component of $\mathbf{v}_{ij}$
v_{sj}	passing velocity of jth interface through double probe
v_{szj}	passing velocity of jth interface through double probe in the z-direction.

Greek symbols

α	void fraction of gas phase
α_j	angle between $\mathbf{v}_{ij}$ and $\mathbf{n}_z$
α_0	limiting value of angle α_j
β_j	angle between $\mathbf{n}_y$ and projection of $\mathbf{v}_{ij}$ into x–y plane
μ_j	angle between $\mathbf{n}_z$ and $\mathbf{n}_j$
ν_j	angle between $\mathbf{n}_j$ and projection of $\mathbf{v}_{ij}$ into x–y plane
ξ_j	angle between $\mathbf{n}_s$ and $\mathbf{n}_j$
σ_z, σ_{sz}	r.m.s. of fluctuating components of $\mathbf{v}_{izj}$, $\lvert v_{szj}\rvert$
τ	average time interval between interfaces
ϕ_j	angle between $\mathbf{n}_j$ and $\mathbf{v}_{ij}$
Ω	time interval of averaging over sampling.

Subscripts

RF	rear sensor signal fall point
RR	rear sensor signal rise point
TF	tip sensor signal fall point
TR	tip sensor signal rise point.

Superscript

$\bar{}$	arithmetic mean.

concentration is essential as shown below. In terms of the mean mass transfer per unit area, m_k, defined by $\Gamma_k \equiv m_k/L_s$, the interfacial energy-transfer term in equation (3) can be rewritten as

$$\Gamma_k H_{ki} + \frac{q''_{ki}}{L_s} = \frac{1}{L_s}(m_k H_{ki} + q''_{ki}). \tag{5}$$

The heat flux at the interface can be modeled using the driving force or the potential for an energy transfer as $q''_{ki} = h_{ki}(T_i - T_k)$ where T_i and T_k are the interfacial and bulk temperatures based on the mean enthalpy and h_{ki} the interfacial heat transfer coefficient. A similar treatment of the interfacial momentum transfer term is also possible. Thus all interfacial transfer terms in the balance equations can be expressed as the product of the local specific interfacial area and the driving force. The driving forces are characterized by the local transport mechanisms such as molecular and turbulent diffusions whereas the local specific interfacial area a_i is related to the structure of the two-phase flow field.

As the above formulation indicates, the knowledge of the interfacial area concentration is indispensable in the two-fluid model. Most of the available experimental data are limited to volume averaged interfacial area concentration over a section of a flow channel. There are very few data available on local measurement of interfacial area concentration. Furthermore, there are few established theoretical foundations for relating this interfacial area to some easily measurable quantities.

Techniques of interfacial area concentration measurement can be broadly classified into two categories: (1) chemical methods for global measurement; (2) physical methods. Detailed reviews of studies carried out with chemical methods in the measurement of interfacial area concentration are given in refs. [3–5]. A number of experimental studies were performed using a chemical absorption technique based on a pseudo-first-order chemical reaction. The volume averaged interfacial area between two sampling points can be measured for a steady state flow without phase changes. Besides their limitation of application for steady state flow without phase change, the chemical techniques do affect the coalescence and disintegration properties of the fluid particles, due to the existence of a surface active agent. This and the very time consuming procedure restrict their applicability. Table 1 outlines the physical methods for determining the interfacial area, including their limitations.

2. THEORY OF LOCAL INTERFACIAL AREA MEASUREMENT FOR DOUBLE RESISTIVITY PROBE

A detailed study of the interfacial area definition using the theory of distribution has been carried out [1]. Among several averages of interfacial area concentration, the time averaged value is most often used for the local interfacial area. The time averaged local interfacial area concentration is given by [1, 21, 22]

$$\bar{a}_i^t = \frac{1}{\Omega}\sum_j \frac{1}{|\mathbf{v}_{ij}|\cos\phi_j} \tag{6}$$

where ϕ_j is the angle between the velocity of the jth

Table 1. Physical methods of measuring interfacial area

Physical methods	Bubble size range (mm)	Limitation problems	References
(1) Photographic method (local and average)	0.1–20	Transparent fluid and walls. Accurate information near focal point	[6–11]
(2) Light transmission (local and average)	1–20	Accurate for low void dispersed phase and transparent systems	[6, 12–15]
(3) Optical probe (local)	1–20	Mechanically sensitive	[16–18]
(4) Ultrasonic pulse transmission (local)	1–20	Low void dispersed phase	[19, 20]
(5) Electrical resistivity probe (local)	0.5–20	Electrically conductive liquid	[9, 21, 33, 34]

interface, $\mathbf{v}_{ij}$, and the direction of the surface normal vector. In equation (6) j stands for all interfaces passing during the averaging period. By denoting the average time interval between interfaces as τ and using the symbol for a mean value, one obtains

$$\bar{a}_t^i = \frac{1}{\tau}\left(\frac{1}{|\mathbf{v}_i| \cos \phi}\right). \tag{7}$$

Now the number of bubbles or droplets which pass the point per unit time is denoted by N_t, then τ can be given by $\tau = 1/(2N_t)$. Here the factor 2 indicates that one particle has two interfaces associated with it. Thus the time averaged interfacial area concentration can be obtained by counting N_t and knowing $|\mathbf{v}_{ij}| \cos \phi_j$ for each interface.

Figure 1 schematically shows a double sensor electrical resistivity probe. Sensors 1 and 2 detect gas and liquid phase by means of the difference between the gas and liquid electrical resistivities. Therefore, using one of these sensors, the number of fluid particles passing the probe per unit time, N_t, can be measured. Furthermore, by measuring the time difference for an interface to pass sensors 1 and 2, the velocity of the interface passing the probe can be measured.

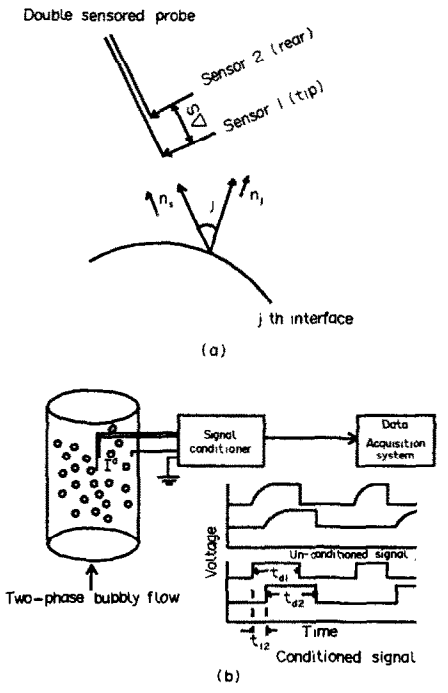

FIG. 1. (a) Double sensor probe and jth interface. (b) Schematic of double probe measurement in two-phase flow system.

Now a double sensor probe oriented in the z-direction is considered where the mean flow is also assumed to be in the z-direction. The velocity and the normal unit vector of the jth interface, $\mathbf{v}_{ij}$ and $\mathbf{n}_j$, can be given in terms of unit vectors $\mathbf{n}_x$, $\mathbf{n}_y$, and $\mathbf{n}_z$, using angles with the z- and y-axes given by (α_j, β_j) and (μ_j, ν_j). By assuming that there are no statistical correlations between $|\mathbf{v}_{ij}|$ and ϕ_j, which is the angle between the interfacial velocity and the direction of the surface normal vector, and that the number of measured interfaces is large, such that the summation can be approximated by a probability integral, it can be shown that [21]

$$\left(\frac{1}{|\mathbf{v}_i| \cos \phi}\right) = \left\{\sum_j \frac{1}{|\mathbf{v}_{ij}|} \Big/ \left(\sum_j\right)\right\} \times \int\int\int\int \frac{P(\alpha, \beta, \mu, \nu)\, d\alpha\, d\beta\, d\mu\, d\nu}{\cos\alpha \cos\mu + \sin\alpha \sin\mu \cos(\beta - \nu)} \tag{8}$$

where $P(\alpha, \beta, \mu, \nu)$ is the probability density function of α, β, μ, ν. The above assumption implies the randomness of either the incident angle ϕ_j or the velocity $\mathbf{v}_{ij}$. For most practical cases of dispersed two-phase flow the first may be assumed.

The above equation indicates that $\bar{a}_i^i$ can be calculated from measured values of the bubble or droplet number, N_t, and of the passing velocity of interfaces using one double sensor probe, if there is no statistical relation between interfacial velocity and the normal vector of the interface [23]. However, in addition to these it is necessary to know the form of the probability density function, $P(\alpha, \beta, \mu, \nu)$. For this purpose, it is assumed that the interfaces are composed of spherical bubbles or droplets and the probe passes every part of the bubble or droplet with an equal

probability. Furthermore, it is assumed that the x- and the y-direction components of $\mathbf{v}_{ij}$ are random. Under these assumptions, β and ν take any value between 0 and 2π with equal probability, and β and ν are statistically independent of each other. By carrying out the probability integral, one obtains

$$\vec{a}_i^t(x_0, y_0, z_0) = 4N_t \left\{\sum_j \frac{1}{|v_{zj}|} \Big/ \left(\sum_j\right)\right\} \times \frac{1}{1 + \dfrac{\int_0^{\pi/2} g(\alpha) \sin\alpha \ln\left(\dfrac{1+\cos\alpha}{\sin\alpha}\right) d\alpha}{\int_0^{\pi/2} g(\alpha)\cos\alpha\, d\alpha}}. \quad (9)$$

Since the main flow is in the z-direction, the major component of the interfacial velocity is also in the z-direction. In that case, $g(\alpha)$ is considered to have a sharp peak at $\alpha = 0$. A simple approximation for $g(\alpha)$ may be given by $g(\alpha) = 1/\alpha_0$ for $0 < \alpha < \alpha_0$ and $g(\alpha) = 0$ for $\alpha_0 < \alpha < \pi/2$. This form of $g(\alpha)$ implies that the angle α made by the interfacial velocity and the z-axis is random with an equal probability within the maximum angle of α_0. Substituting this relation into equation (9), the interfacial area concentration becomes

$$\vec{a}_i^t = \frac{4N_t \left\{\sum_j \dfrac{1}{|v_{zj}|} \Big/ \left(\sum_j\right)\right\}}{1 - \cot\frac{\alpha_0}{2} \ln\left(\cos\frac{\alpha_0}{2}\right) - \tan\frac{\alpha_0}{2} \ln\left(\sin\frac{\alpha_0}{2}\right)}. \quad (10)$$

Therefore, by knowing the value of α_0, the time averaged local interfacial area concentration can be calculated from the measured values of N_t and v_{zj}.

The value of α_0 can be estimated from the measured values of statistical parameters of the interfacial velocity [23]. The result shows that α_0 is related to the mean characteristic of the turbulent motion of the interface as

$$\frac{\sin 2\alpha_0}{2\alpha_0} = \frac{1 - (\sigma_z^2/|\overline{\mathbf{v}_{iz}}|^2)}{1 + 3(\sigma_z^2/|\overline{\mathbf{v}_{iz}}|^2)}. \quad (11)$$

In deriving equation (11) it is assumed that the r.m.s. of the fluctuations of the z component interfacial velocity, σ_z, is equal to that of the r.m.s. of the x and y component velocity fluctuations. The study [24] carried out for bubbly flow in a vertical pipe using the ultrasonic Doppler technique, has shown that the magnitude of the axial component the r.m.s. bubble velocity fluctuation is nearly equal to the transverse components of the r.m.s. of the fluctuations of bubble velocity. Then by knowing $|\mathbf{v}_{iz}|$ and σ_z, it is possible to estimate the value of α_0.

3. DOUBLE SENSOR RESISTIVITY PROBE METHOD

3.1. *Principle of measurement*

The electrical resistivity probe technique was proposed by Neal and Bankoff [25] for determination of bubble size and velocity in gas–liquid bubbly flows. Since then the double resistivity probe has been used by Park *et al.* [26], and Rigby *et al.* [27] for the determination of bubble parameters in three-phase fluidized beds, by Hoffer and Resnick [28] for steady and unsteady state measurements in liquid–liquid dispersions, by Burgess and Calderbank [29] for the measurement in single bubbly flow, by Serizawa *et al.* [30], and Herringe and Davis [31] for the study of the structural development of gas–liquid bubbly flow. Resistivity probes have also been used by Veteau [9], Sekoguchi *et al.* [32], Kataoka and Serizawa [33], and Buchholz *et al.* [34] to measure bubbly flow characteristics and the local specific interfacial area in gas–liquid systems. In early works employing the double resistivity probe in bubbly flow the transverse bubble velocities have been neglected in measuring the interfacial area. However, the theoretical study carried out at Argonne [21] indicated that the effect of the bubble transverse fluctuations affects the interfacial area and should be included in the formulation. Recently a double sensor resistivity probe was used by Wang and Kocamustafaogullari [35] in a horizontal test pipe and by Kataoka and Serizawa [36] in a vertical test pipe for the measurement of local interfacial parameters for an air–water bubbly flow system. Basically these investigators used the same theoretical formulation developed in ref. [23] to determine the interfacial area concentration in bubbly flow employing a double resistivity probe.

In order to apply the double sensor probe method, electrical resistivity probes have been used. The method is based on the instantaneous measurement of local electrical resistivity around a sensor in the two-phase system by a double sensor electrode. The measurement principle is illustrated in Fig. 1. Sensors are made of an exposed tip of an otherwise electrically insulated metal wire. Basically each sensor works independently as an identifier of a phase surrounding that tip. As the circuit is opened or closed depending on whether the sensor is in contact with gas or liquid, the voltage drop across the sensor fluctuates between two reference voltages. For liquid continuous two-phase flow such as bubbly flow, the circuit is closed when the sensor is in liquid.

In the double sensor probe technique, each sensor is used independently as a phase identifying device. Furthermore, from the timing of the shift in the voltage, the time when the gas–liquid interface passes the sensor can be recorded. Therefore, parallel and independent information related to the phase identification and the passing time of the gas–liquid interface is obtained through the signal conditioner from two closely located sensors. The typical time history records of signals from a double sensor electrical resistivity probe in bubbly flow is shown in Fig. 2.

As indicated in Fig. 1, the unconditioned signal shows a near exponential rise of the signal as the bubble hits the electrode. This is due to the finite size of the sensor and the possible deformation of the

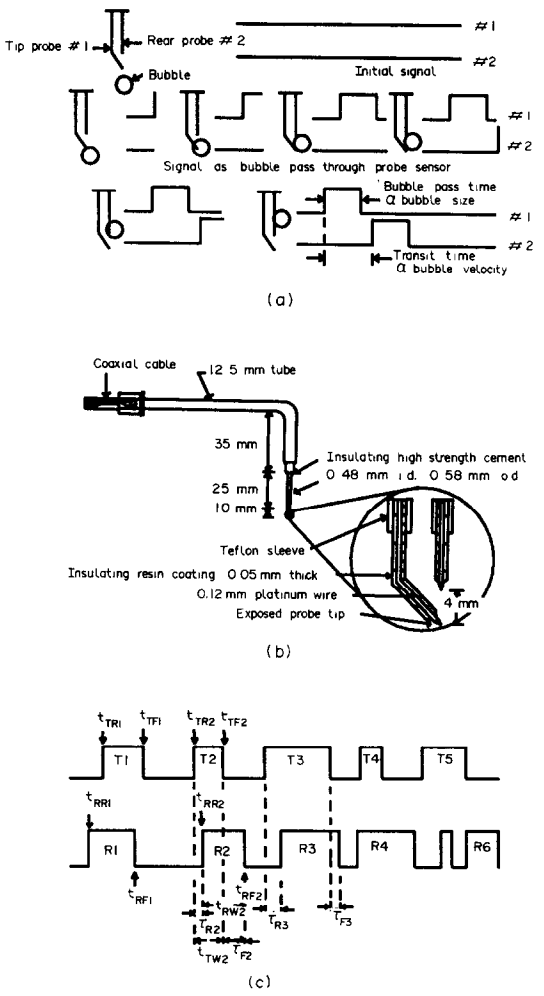

FIG. 2. (a) Signal as a single bubble passes through double resistivity probe. (b) Design of typical resistivity probe. (c) Double probe tip and rear sensor signal tagging.

interface. The trailing edge of the signal is steeper than the leading edge. In addition to these there is inherent noise in the signal. In order to condition the voltage output to ideal square wave type signals, a proper threshold voltage has to be used as a triggering criterion. The value of the threshold voltage can be obtained by processing the data for the void fraction and by comparing the data with other reference measurement methods, such as the photographic technique. The threshold voltage can be determined by a calibration procedure where measurements and signal processing are done on a bubble whose size and frequency are optically recorded and the data are compared with the double sensor probe technique. In the present study, it was sufficient to set the threshold voltage just above the circuit noise level so that clean square signals were obtained. Hence two different threshold levels are used.

The void fraction data can be obtained from either of the two sensors. The cross check between them and against other global methods such as the photographic and Δp transducer techniques used in the present work, assured that either the tip or rear sensor signal was independently suitable for void fraction data. The signals from these two sensors are used to measure the interface velocity by comparing the two passing timings (from the tip and rear sensors) belonging to the same interface. From the known distance between the sensors, the interface velocity is calculated using these timings.

In the double sensor probe technique, the direction of the two sensor points is made to coincide with the axial flow direction. In this case, an additional information on the transverse velocity fluctuation of bubbles is needed as explained in the section describing the mathematical principle. In the previous work of Kataoka *et al.* [23], the hot-film measurement of the liquid turbulence has been used for this purpose. However, in the present study the fluctuation of the axial bubble velocity measured directly by the resistivity probe has been used. This is considered to be a major improvement because:

(1) the measured bubble velocity fluctuations are used instead of liquid velocity fluctuations;

(2) no additional measurement such as the hot-film anemometer is required.

3.2. *Double sensor probe design*

A typical double sensor resistivity probe design is shown in Fig. 2. The material for the probe conductor is platinum wire of diameter 0.12 mm. The platinum wires were first insulated with GE No. 7031 adhesive and insulating varnish and then inserted into a 0.5 mm i.d. stainless steel tube with 5 min epoxy resin for sealing and bonding. The 0.5 mm i.d. tube was inserted in another ss tube of 1.04 mm i.d. which in turn was inserted in a 1.8 mm i.d. ss tube. The tips of the two electrodes were adjusted for typical spacings of 2–5 mm in the lengthwise direction and were aligned in the axial direction. The other end of the probe electrode was connected to copper wires. The whole probe assembly was put in a 3.175 mm tube which has a 90° elbow bend. A high strength epoxy resin cement was used to hold one tube to the other. The probe tips were left exposed and a final coating of epoxy resin was applied to insulate the rest of the probe conductor electrodes.

3.3. *Signal processing*

As the conditioned signals for bubbly flow consist of a train of square waves from both probes, the signal has to be processed such that the number of bubbles passing through the probe location and the bubble velocity information can be obtained by selecting the gas or liquid phase residence times with either probe sensor. For measurement of bubble number the tip probe signal is utilized. The total number of squares detected would give the number of bubbles hitting the tip sensor in a given period of time. Also the width of

each square is the bubble residence time. This information gives the time averaged local void fraction.

For the case of the bubble velocity measurement the right selection of two closely corresponding signals from each probe is important, because two sequential signals detected by both sensors do not always correspond to the same interface, and the residence time intervals of the gas or liquid phase at the sensors are not exactly the same. The signal validation was made by judging whether the following conditions were satisfied (Fig. 5):

(1) By assuming the forward motion of the bubbles the tip sensor signal rises or falls before the rear sensor signal does. Therefore, denoting the times of the rise and fall in the tip and rear sensor signals by t_{TRi}, t_{TFi}, t_{RRi} and t_{RFi}, respectively, the condition is given as

$$t_{TRi} < t_{RRi} \quad \text{and} \quad t_{TFi} < t_{RFi}. \tag{12}$$

(2) The residence time of a bubble in the tip and rear sensors should be comparable (30%) to ensure that both sensors detect the same bubble. Hence the width of the square wave signals from both sensors which satisfy the first condition should also satisfy the following condition:

$$\left| \frac{(t_{TFi} - t_{TRi}) - (t_{RFi} - t_{RRi})}{(t_{TFi} - t_{TRi})} \right| \leqslant 0.3. \tag{13}$$

(3) The difference between the tip and rear sensor timing scaled by $t_{TRi} - t_{TFi}$ should be limited by the condition

$$C_1 < (t_{TRi} - t_{TFi}) < C_2 \tag{14}$$

where C_1 and C_2 are the time limits assigning maximum and minimum velocity of the bubble and are determined during the calibration procedure based on the liquid and gas volumetric fluxes and using a drift flux model.

(4) For the bubbles hitting the tip sensor but missing the rear sensor, it is necessary to compensate for the missed interfacial area contribution. This is clear from the discussion of void fraction signals. The interfacial velocity for these bubbles was taken as the average velocity determined from the bubbles that hit both the tip and rear sensors of the double probe.

4. EXPERIMENTAL APPARATUS AND PROCEDURES

A schematic diagram of the experimental apparatus is shown in Fig. 3. The test section is made of lucite pipe. The height of the test pipe is 1.5 m and its inside diameter is 0.0508 m. The bubble generator was made of 49 stainless steel hypodermic tubes of 0.12 mm i.d. The tubes were arranged in a 7×7 square matrix with a pitch of 0.007 m and were supported by a high strength epoxy cement plate. This plate consisting of vertically arrayed tubes is used as the gas injection nozzles between the air plenum and the water column.

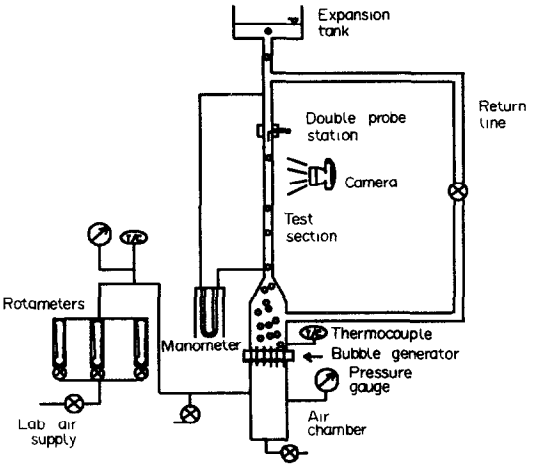

FIG. 3. Schematic of bubble column experimental set-up.

The bubble generator produces uniform size bubbles. Demineralized water was used for the experiment. The double sensor probe was mounted on the traversing mechanism made of a micrometer screw gauge. In the present measurements the probe was stationed at 1.1 m from the inlet of the test section. Using the traversing mechanism, the double probe can be moved radially from the center towards the pipe wall up to 2.5 mm from the wall. A camera was mounted slightly upstream of the double probe station. A strobe lighting system giving exposure of a few microseconds was used along with the Nikon camera system for still photography. The data acquisition systems consisted of a fast A/D converter Metrabyte DAS-20 board and an IBM/PC-XT computer. The DAS-20 is capable of handling 100 000 samples per second. In the experiment the superficial gas flow rate was varied from 0 to 0.12 m s^{-1}. The return line was closed, hence the superficial liquid velocity was zero.

For each gas flow rate the double sensor probe measurements were taken for the radial profiles of the interfacial velocity, void fraction and interfacial area, and the optical measurements were made through still photography. An accurate measurement of the two-phase pressure drop in the test section was converted to two-phase gravitational head to obtain the global void fraction data. Note, under the present experimental conditions the frictional loss was almost completely negligible in comparison with the head loss.

Additional experiments were also conducted in the forced flow air–water flow test facility to see the effect of liquid flow rate on the measurements of interfacial area concentration in bubbly flow. This test loop consisted of a 0.0508 m diameter lucite pipe of length 3.73 m. The location of the double resistivity probe on this test section was at 3.1 m from the inlet. Bubbles were generated by a porous sintered metal tube and were mixed with the water that flows through a conical shape entrance to the inlet of the test section.

5. EXPERIMENTAL RESULTS AND DISCUSSION

The data on various bubble parameters were obtained from the bubble column test loop for the superficial gas velocity ranging from 0.0034 to 0.1212 m s^{-1}. For the forced flow test loop the superficial liquid velocity was varied from 0.1 to 1 m s^{-1} with the superficial gas velocity of 0.0675 m s^{-1}. Typical void fraction profiles obtained in the bubble column are presented in Fig. 4, where the void fraction measurements from both the tip and rear sensors are shown. Here the non-dimensional distance from the wall is defined as the ratio between the distance of the tip sensor from the pipe wall and the radius of the pipe (r/d). From these figures it is clear that some bubbles that hit the tip sensor do not hit the rear sensor. This occurs due to the finite distance between the tip and rear sensor. Also at low gas injection rates fewer bubbles hit both the sensors. Since for the interface velocity measurement the transit time of the interface between the tip and rear sensor is required, it is essential that longer data sampling time is necessary for low gas flow rates to get enough velocity measurements. For the local void fraction measurement either tip or rear sensor data were independently adequate as shown in Fig. 4.

The measured profiles of the local void fraction at various gas injection rates are shown in Fig. 5. The void fraction values are nearly constant in the radial directions except near the wall where these values decrease toward zero at the wall. However, in some cases a local peaking of the void fraction can be observed near the wall. In order to validate the double probe data comparisons with other global measurement methods were made. For this purpose the differ-

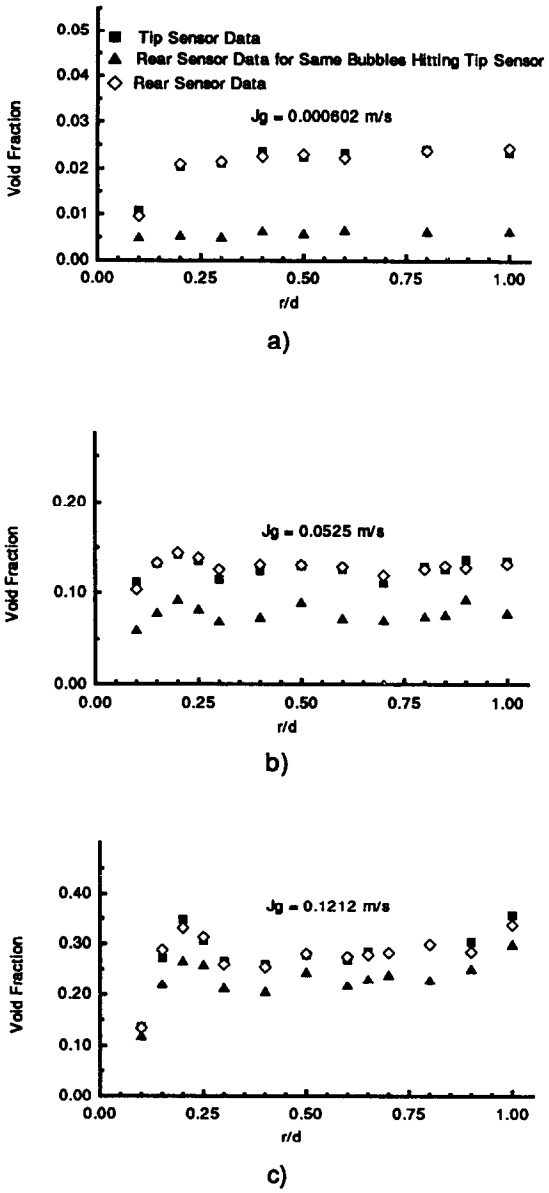

FIG. 4. Comparison of void fraction measurement from the tip and rear sensor of a double probe for: (a) j_g = 0.0060 m s^{-1}; (b) j_g = 0.0525 m s^{-1}; (c) j_g = 0.1212 m s^{-1}.

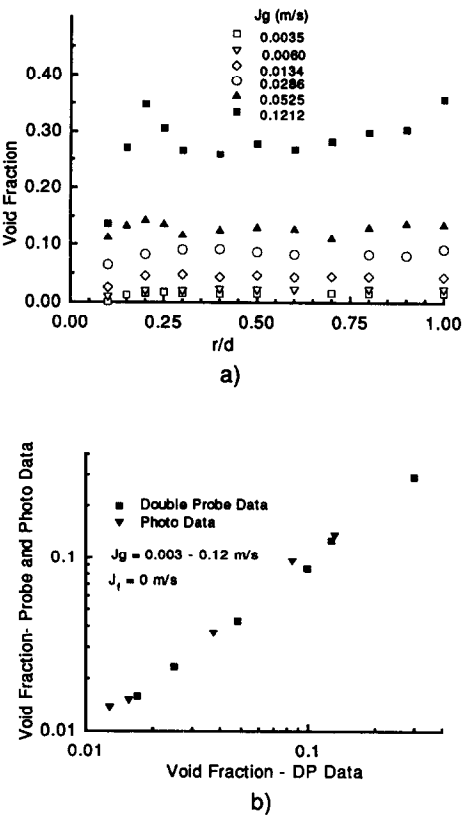

FIG. 5. (a) Radial void fraction profiles for different gas injection rates. (b) Comparison of average void fraction obtained from double resistivity probe, differential pressure and photographic measurements in bubble column.

ential pressure measurement data were utilized. As shown in Fig. 5 the void fraction obtained from the differential pressure measurement compared very well with those obtained from the double sensor probe measurement.

In the measurement of velocity the double sensor probe in effect measures the interface velocity. The mean velocity of the front interface of the bubble is taken as the mean axial velocity of the bubble. Here it should be noted that for large and non-spherical bubbles this assumption may lead to considerable error. In the present study the bubbles were of small sizes (average diameter $\leqslant 5$ mm) and near spherical shape. Data of the mean bubble axial velocity profiles are shown in Fig. 6 for various gas injection rates. The local velocity profiles show basically the power law profile with the maximum at the pipe center at all gas injection rates. This mean axial bubble velocity represents the most probable axial velocity of the bubble. A typical bubble velocity distribution in terms of probability density functions are presented in Fig. 6 at different radial positions. Based on these velocity spectra the r.m.s. of the bubble velocity fluctuations were obtained. The standard deviations from mean axial bubble velocity varied from 0.037 to 0.11 m s^{-1} for the range of the gas superficial velocity studied. Figure 6 shows the radial profiles of the r.m.s. of the fluctuations in the bubble velocity. The axial fluctuating component over the mean bubble velocity generally increased with an increase in the superficial gas velocity except for high gas flow rates ($j_g = 0.1212$ m s^{-1}). This occurs probably due to large void fraction observed at high gas flow rate. At large gas flow rates the void fraction was almost 30% as shown in Fig. 5. This flow rate corresponds very closely to the transition zone from the bubbly to the slug flow regime.

The radial profiles of the bubble chord length are presented in Fig. 7. Here the bubble chord length is defined as the product of the bubble velocity and the bubble transit time through the sensor. Hence it is related to the bubble size. The probability density of the chord length is related to the bubble diameter distribution if the following assumptions are made. The bubbles are spherical, all bubbles travel in the same direction with the same average velocity, and the probe has equal probability to pierce any point on the projected frontal area of the bubble. Typical bubble chord length distributions in terms of the probability density function are shown in Fig. 7. It should be noted that the distribution functions and mean diameters obtained are the representation of the detected bubbles. In terms of the governing equations for heat and mass transfer in two-phase flow the interfacial area is more important rather than the bubble mean diameter. Hence it would be more convenient to use the Sauter mean diameter to define the bubble size. The Sauter mean diameter is based on the bubble interfacial area and the void fraction as defined later in this section.

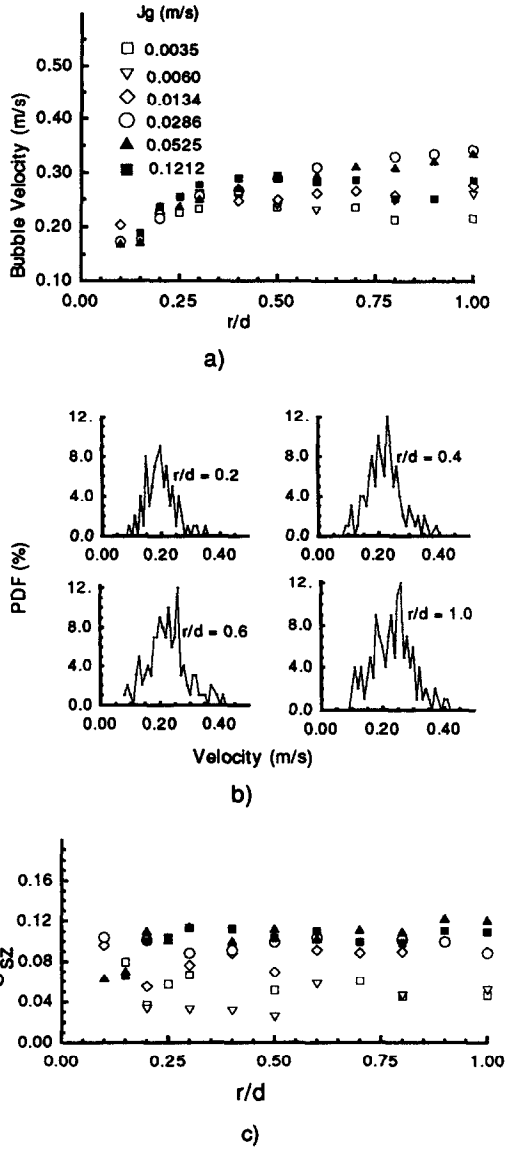

FIG. 6. (a) Radial bubble velocity profiles for different gas injection rates. (b) Probability density functions for bubble velocity measured with double probe at different radial position for $j_g = 0.0060$ m s^{-1}. (c) Radial profiles of r.m.s. of the bubble velocity fluctuation for different gas injection rates.

The local interfacial area concentration a_i was calculated from equations (10) and (11). The r.m.s. of the fluctuations of the interface velocity was used to calculate the angle α_0 in equation (11). Using this angle α_0, the inverse mean interface velocity and the total number of bubbles detected N_t, the interfacial area concentration a_i was calculated from equation (10). For the bubbles that miss the rear sensor of the double probe the interfacial area concentration was calculated using the inverse mean interface velocity obtained with the bubbles that hit the tip and rear sensors. The radial profiles of local interfacial area concentration are shown in Fig. 8 for different gas

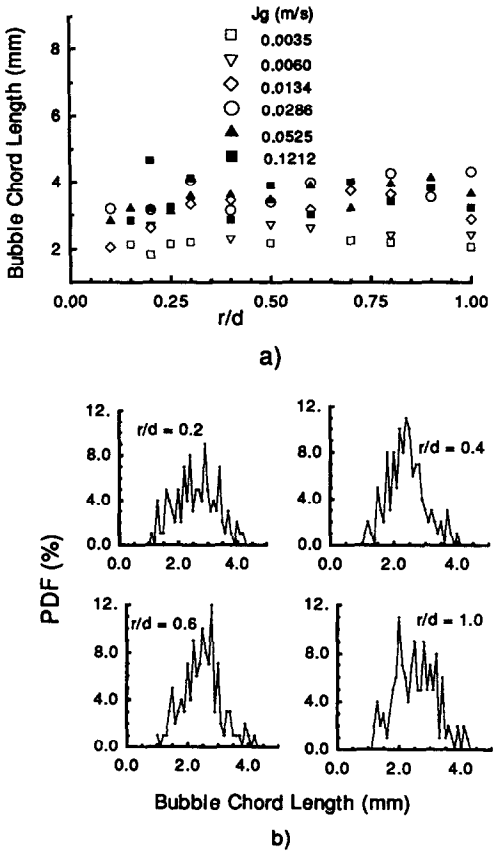

FIG. 7. (a) Radial profiles of bubble chord length obtained with probe measurement for different gas injection rates. (b) Probability density functions for bubble chord length measured with double probe at different radial position for $j_g = 0.0060$ m s^{-1}.

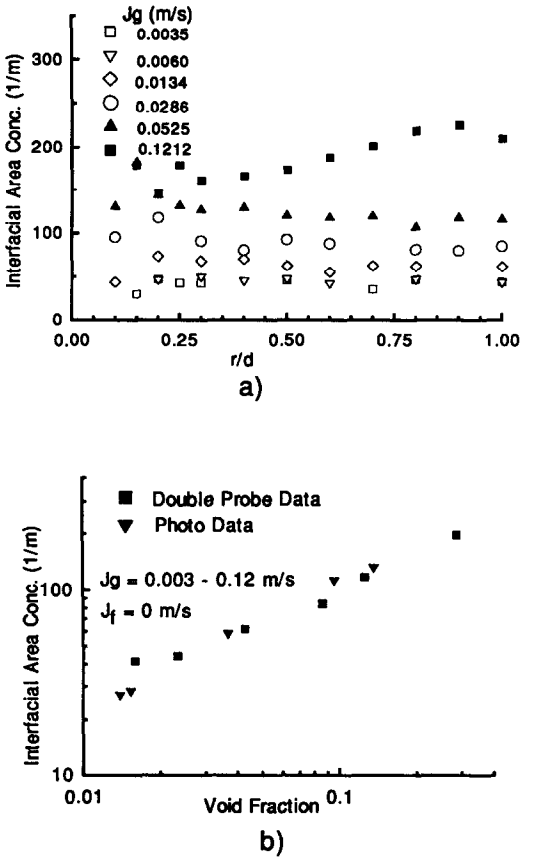

FIG. 8. (a) Radial profiles of interfacial area concentration in bubble column for different gas injection rates. (b) Average interfacial area concentration as a function of void fraction and comparison of double probe data with photographic data for bubble column.

injection rates. It can be seen that the profiles of the local interfacial area concentration are almost flat except near the wall for low gas injection rates ($j_g \leqslant 0.0134$ m s^{-1}). At intermediate gas injection rates (0.0134 m s^{-1} $\geqslant j_g \geqslant$ 0.0525 m s^{-1}) the values of the local interfacial area concentration tend to have a saddle shape and reach a maximum near the wall. However, for large gas injection rates ($j_g \geqslant 0.1212$ m s^{-1}) the profile shows two peaks; one near the wall and the other at the centerline. Comparing the local void fraction profiles (Fig. 5) and the local interfacial area concentration profiles (Fig. 8) it can be seen that the void fraction and the interfacial area concentration profiles show similar shapes. This complementary nature of the void fraction and the interfacial area concentration profiles was also observed by Wang and Kocamustafaogullari [35] in their horizontal test section. However, the void fraction and interfacial area concentration profiles observed by the latter authors were different compared to the present profiles, where a local maximum was observed near the upper side of the horizontal pipe.

By area averaging the local a_i profile, the average interfacial area concentration was obtained. In Fig. 8 the average interfacial area concentration is shown as a function of the average void fraction. The interfacial area concentration is strongly affected by the bubble sizes, since the surface to volume ratio of a small bubble is larger than that of a larger bubble. Furthermore, when the bubbles are not spherical, this ratio also depends on the shape of the bubble at the same void fraction. In general the spherical shape gives the minimum surface area.

The Sauter mean diameter D_{vs} is given by $D_{vs} \equiv 6\alpha/a_i^1$. It is also related to the volume mean diameter D_v and the surface mean diameter D_s by $D_{vs} = D_v^3/D_s^2$. Thus the larger the interfacial area, D_{vs} becomes smaller. Based on the above relations the Sauter mean diameter was calculated. The radial profiles of the Sauter mean radius at various gas fluxes and the area averaged Sauter mean diameter are shown in Fig. 9. The Sauter mean diameter is based on the equivalent interfacial area concentration at the same void fraction.

Photographs of bubble flow were taken at five different gas injection rates. The pictures were pro-

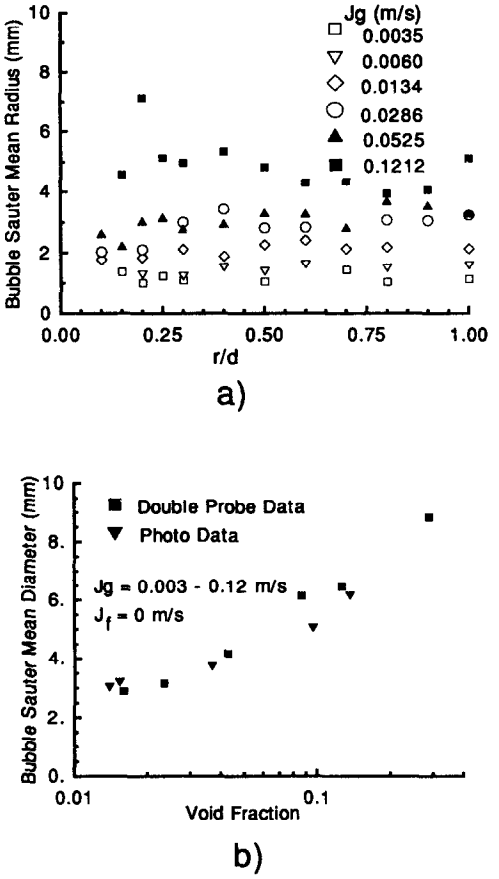

FIG. 9. (a) Radial profiles of Sauter mean radius of bubbles obtained with probe measurement for different gas injection rates. (b) Average bubble Sauter mean diameter as a function of void fraction and comparison of double probe data with photographic data for bubble column.

jected on a paper with a slide projector and the projections of bubble shapes were traced on the paper. The shape of the bubble resembled somewhere between ellipsoidal and spherical. In order to estimate the surface area and the volume of each bubble, the maximum axis length b and the minimum axis length a were measured for each bubble in a designated volume sample. The surface area of the jth bubble was calculated as

$$A_j = \frac{\pi}{2}(b-a)(\pi a + b - a)$$

assuming the rotational ellipsoid. The volume of the jth bubble was calculated as

$$V_j = \frac{\pi}{6}ab^2.$$

From these, void fraction and interfacial area have been obtained. From the ergodic theorem [23], the volume average of the local time averaged interfacial area concentration should be equal to the time average of the volume averaged value for a stationary flow. The summary of the results of photographic measurements is shown in Table 2. The average void fractions obtained by photographic measurement agree very well with that obtained from differential pressure measurement (see Fig. 5). Figure 10 shows the comparison of the interfacial area concentration data obtained from the photographic measurements with those obtained from the double sensor probe method.

The Sauter mean diameter of bubbles obtained from the photographic measurement shows slightly smaller values when compared with double sensor probe measurement at a void fraction $\alpha > 0.02$ (see Fig. 9). The discrepancy is expected since, for non-spherical bubbles, such as in the present case, the evaluation of the photographic images involves interpretation of two-dimensional images to three-dimensional shapes of particles. The formulas used to calculate the volume and surface area of a bubble tend to give a larger surface area to volume ratio. Thus this may lead to underestimation of the Sauter mean diameter and overestimation of interfacial area. But the overall agreement between the photographic measurements and the double probe measurement of average interfacial area concentration (Fig. 8) and the averaged void fraction (Table 2) validates the double sensor probe measurement techniques.

Results of the measurements using a double resistivity probe in the forced flow air–water loop are shown in Fig. 11. The local void fraction profiles show that the void fraction decreases with an increase in the liquid flow rate for a given gas injection rate. The void fraction near the wall and near the center of the pipe is slightly larger than the bulk average. The interfacial area concentration shows that the average interfacial area concentration decreases with an increase in liquid flow rate for the same gas flow rate. A similar behavior, namely an increase in the liquid flow rate at constant gas flow, would decrease the local void fraction and the interfacial area concentration was also observed by Kataoka and Serizawa [36] and by Wang and Kocamustafaogullari [35] in vertical and horizontal test sections respectively. Typically the average interfacial area concentration values in the present forced flow experiments ranged from 70 to 125 l m^{-1} for the superficial liquid velocity from 0.1 to 1 m s^{-1} with the superficial gas velocity in the test section at 0.0675 m s^{-1}.

6. CONCLUSIONS

The survey of the previous works show that very few data exist on the local interfacial area concentration for two-phase flow systems. A method of measurement of the local interfacial area concentration using a double sensor resistivity probe has been described for the bubbly flow system. This method is based on the local instantaneous formulation of the interfacial area concentration, where the time averaged value of the latter parameter is given in terms of the number of interfaces per unit time and the harmonic mean of $|\mathbf{v}_{ij}\cos\phi_j|$, where $\mathbf{v}_{ij}$ is the

Table 2. Results of photographic measurement

Set No.	j_g (cm s^{-1})	Average void fraction α	Total No. of bubbles	Total surface area (cm^2)	Volume mean D_v (cm)	Total volume (cm^3)	Sauter mean D_{vs} (cm)	Void fraction α	Interfacial area (cm^{-1})
1	0.277	0.0128	263	65.060	0.280	3.33410	0.307	0.01389	0.271
2	0.338	0.0156	281	67.015	0.276	3.6079	0.323	0.01529	0.284
3	1.052	0.0375	295	136.921	0.384	8.616	0.376	0.0368	0.586
4	2.723	0.0851	350	287.630	0.465	20.198	0.508	0.096	1.132
5	4.334	0.1321	385	269.908	0.472	27.846	0.619	0.1367	1.325

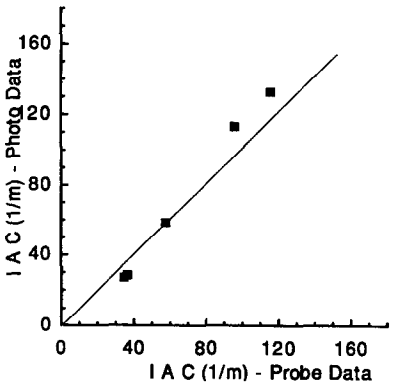

FIG. 10. Comparison of average interfacial area concentration data from photographic and double probe measurements.

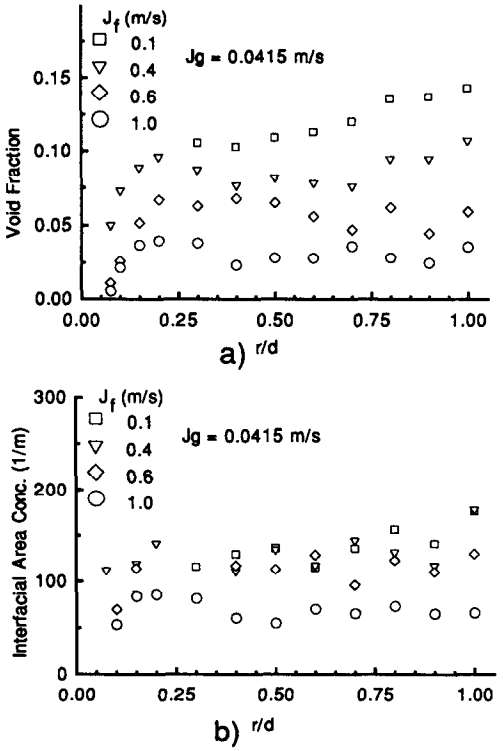

FIG. 11. (a) Radial profiles of void fraction for bubbly flow in forced flow air–water loop for different liquid flow rates at $j_g = 0.0675$ m s^{-1}. (b) Radial profiles of interfacial area concentration for bubbly flow in forced flow loop for different liquid flow rates at $j_g = 0.0675$ m s^{-1}.

interfacial velocity of the jth interface and ϕ_j the angle between $\mathbf{v}_{ij}$ and the normal vector of the jth interface. By assuming certain statistical characteristics of the interfacial motion, an expression for the local interfacial area concentration has been related to measurable quantities from a double sensor probe.

Details of the double resistivity probe measurement method have been presented for a bubbly two-phase system including the probe design and the data processing. Applying this double sensor probe to air–water bubbly flow in a vertical test section, the radial profiles of the void fraction, bubble velocity, bubble chord length and interfacial area concentration have been obtained for different gas injection rates with negligible liquid flow. In order to validate the double sensor probe data, two independent global measurement methods, namely, differential pressure and photographic methods were employed. A good agreement was found between the global measurements and the double sensor probe measurement of the average void fraction, average interfacial area concentration and Sauter mean diameter of bubbles.

The results of the radial void fraction profiles showed that the void fraction values were nearly constant in the radial direction except near the wall where these values decreased toward zero at the wall. However, for large gas flow rates a local peaking of the void fraction was observed near the wall. The local bubble velocity profiles showed basically a power law profile with the maximum at the pipe center.

The shape of the radial profiles of the interfacial area concentration showed dependence on the gas injection rate. At low injection rates ($j_g \leqslant 0.0134$ m s^{-1}) the profile was almost flat except near the wall where it decreased rapidly to zero. At intermediate gas injection rates (0.0134 m s$^{-1} \geqslant j_g \geqslant 0.0525$ m s^{-1}) the profile showed a peak near the wall, whereas, at large gas injection rates ($j_g \geqslant 0.1212$ m s^{-1}) the profile showed two peaks, one near the wall and the other at the centerline. The peaking of interfacial area concentration profiles near the wall complement the void fraction profiles for larger gas injection rates ($j_g \geqslant 0.0525$ m s^{-1}). This indicates the higher concentration of bubbles near the wall.

Further experimental study with the double sensor probe was conducted in another air–water vertical test facility where the effect of liquid flow rate on the interfacial area concentration was studied. Some pre-

liminary results on the measurement of the interfacial area concentration profiles in the forced flow condition for different liquid flow rates were presented. These profiles showed that with an increase in the liquid flow rate the average interfacial area concentration decreases at the same gas flow rate.

Acknowledgements—This work was performed under the auspices of U.S. Department of Energy, Office of Basic Energy Science. The authors would like to express their sincere appreciation for the encouragement, support and technical comments on this program from Drs O. P. Manley and M. C. Yuen (currently at Northwestern University) of DOE/BES.

REFERENCES

1. M. Ishii, *Thermo-fluid Dynamic Theory of Two-phase Flow*. Eyrolles, Paris, Scientific and Medical Publication of France, New York (1975).
2. J. M. Delhaye, Equations fondamentales des écoulements disphasiques, Parts 1 and 2, CEA-R-3429, France (1968).
3. M. Ishii and K. Mishima, Study of two-fluid model and interfacial area, Argonne National Laboratory Report ANL-80-111, NUREG/CR-1873 (1980).
4. M. Ishii and K. Mishima, Two-fluid model and hydrodynamic constitutive relations, *Nucl. Engng Des.* **82,** 107–126 (1984).
5. G. Kocamustafaogullari and M. Ishii, Interfacial area and nucleation site density in boiling systems, *Int. J. Heat Mass Transfer* **26,** 1377–1387 (1983).
6. J. Landau, J. Boyle, H. G. Gomaa and A. M. Al Tawell, Comparison of methods for measuring interfacial areas in gas–liquid dispersions, *Can. J. Chem. Engng* **55,** 13–28 (1977).
7. A. Schumpe and W. D. Deckwer, Comparison of the photographic and the sulfite oxidation method for interfacial area determination in bubble columns, *Chem. Engng Commun.* **17,** 213–324 (1982).
8. K. Akita and F. Yoshida, Bubble size, interfacial area, and liquid-phase mass transfer coefficient in bubble columns, *Ind. Engng Chem. Process Des. Dev.* **13,** 84–91 (1974).
9. J. M. Veteau, Contribution à l'études des techniques de mesure de l'aire interficiale dans les écoulements d'bulles, Sc.D. Thesis, National Grenoble Polytechnic Institute, France (1981).
10. J. J. Jeng, R. M. Jer and Y. M. Yang, Surface effects and mass transfer in bubble column, *Ind. Engng Chem. Process Des. Dev.* **25,** 974–978 (1986).
11. N. S. Yang, Z. Q. Shen, B. H. Chen and A. F. McMillan, Pressure drop, gas holdup, and interfacial area for gas–liquid contact in Karr columns, *Ind. Engng Chem. Process Des. Dev.* **25,** 660–664 (1986).
12. T. Sridhar and O. E. Potter, Interfacial area measurements in gas–liquid agitated vessels, comparison of techniques, *Chem. Engng Sci.* **33,** 1347–1353 (1978).
13. P. H. Calderbank, Physical rate processes in industrial fermentation, Part I: the interfacial area in gas–liquid contacting with mechanical agitation, *Trans. Inst. Chem. Engng* **36,** 443–463 (1958).
14. C. M. McLaughlin and J. H. Rushton, Interfacial area of liquid–liquid dispersions from light transmission measurements, *A.I.Ch.E. Jl* **19,** 813–822 (1973).
15. T. Sridhar and O. E. Potter, Interfacial areas in gas–liquid stirred vessels, *Chem. Engng Sci.* **35,** 683–695 (1980).
16. N. Miller and R. E. Mitchie, Measurement of local voidage in liquid/gas two phase flow systems using a universal probe, *J. Br. Nucl. Energy Soc.* **9,** 94–100 (1970).
17. J. P. Galaup and J. M. Delhaye, Utilisation de sondes optiques miniatures en écoulement diphasique gaz–liquide, *La Houille Blanche* No. 1, 17–30 (1976).
18. P. H. Calderbank and J. Pereira, The prediction of distillation plate efficiencies from froth properties, *Chem. Engng Sci.* **32,** 1427–1433 (1977).
19. A. A. Stravis, U. Von Stockar and P. J. Reilly, Measurement of interfacial areas in aerobic fermentations by ultrasonic pulse transmission, *Biotech. Bioengng* **28,** 1302–1309 (1986).
20. H. P. Bensler, J. M. Delhaye and C. Favreau, Measurement of interfacial area in bubbly flows by means of an ultrasonic technique, paper presented at the 24th ASME/AIChE Natn. Heat Transfer Conf., Pittsburgh, Pennsylvania, 9–12 August (1987).
21. I. Kotaoka, M. Ishii and A. Serizawa, Local formulation of interfacial area concentration, *Int. J. Multiphase Flow* **12,** 505 529 (1986).
22. J. M. Delhaye, Sur les surfaces volumiques locale et integrale en écoulement disphasiques, *C.R. Acad. Sci.* **A282,** 243–246 (1976).
23. I. Kataoka, M. Ishii and A. Serizawa, Local formulation of interfacial area concentration and its measurements in two-phase flow, Argonne National Laboratory Report ANL-84-68, NUREG/CR-4029 (1984).
24. W. Hilgert and H. Hofmann, Characterization of gas phase flow in bubble columns at low superficial gas velocities with the aid of ultrasonic Doppler techniques, *Ger. Chem. Engng* **9,** 180–190 (1986).
25. L. G. Neal and S. G. Bankoff, A high resolution resistivity probe for determination of local void properties in gas–liquid flow, *A.I.Ch.E. Jl* **9,** 490–494 (1963).
26. W. H. Park, W. K. Kang, C. E. Capes and G. L. Osberg, The properties of bubbles in fluidized beds of conducting particles as measured by an electroresistivity probe, *Chem. Engng Sci.* **24,** 856–865 (1969).
27. G. R. Rigby, G. P. Van Blockland, W. H. Park and C. E. Capes, Properties of bubbles in three phase fluidized beds as measured by an electrosensitivity probe, *Chem. Engng Sci.* **25,** 1729–1741 (1970).
28. M. S. Hoffer and W. Resnick, A modified electroresistivity probe technique for steady- and unsteady-state measurements in fine dispersions—I. Hardware and practical aspects, *Chem. Engng Sci.* **30,** 473–480 (1975).
29. J. M. Burgess and P. H. Calderbank, The measurement of bubble parameters in two-phase dispersions—I. The development of an improved probe technique, *Chem. Engng Sci.* **30,** 743–750 (1975).
30. A. Serizawa, I. Kataoka and I. Michiyoshi, Turbulence structure of air–water bubbly flow—I. Measuring techniques, *Int. J. Multiphase Flow* **2,** 221–233 (1975).
31. R. A. Herringe and M. R. Davis, Structural development of gas–liquid mixture flows, *J. Fluid Mech.* **73,** 97–123 (1976).
32. K. Sekoguchi, H. Fukui, M. Tsutsui and K. Nishikawa, Investigation into the statistical characteristics of bubbles in two-phase flow (2nd Report, Application and establishment of electrical resistivity probe method), *Bull. JSME* **18,** 397–404 (1975).
33. I. Kataoka and A. Serizawa, Averaged bubble diameter and interfacial area in bubbly flow, *Proc. 5th Two-phase Symp. Japan*, Kobe, Japan, 28–29 November, pp. 77–80 (1984).
34. R. Buchholz, J. Tsepetonides, J. Steinemann and U. Onken, Influence of gas distribution on interfacial area and mass transfer in bubble columns, *Ger. Chem. Engng* **6,** 105–113 (1983).
35. Z. Wang and G. Kocamustafaogullari, Interfacial characteristic measurements in a horizontal bubbly two-phase flow, *Trans. ANS* **62,** 712–713 (1990).
36. I. Kataoka and A. Serizawa, Interfacial area concentration in bubbly flow, *Nucl. Engng Des.* **120,** 163–180 (1990).

MESURE LOCALE DES AIRES D'INTERFACE DANS UN ECOULEMENT A BULLES

Résumé—On présente les bases théoriques de la méthode de mesure des aires d'interface locales moyennes dans le temps en utilisant une sonde double. Des données expérimentales sont présentées pour les profils radiaux, à différents débits gazeux, de fraction de vide, de vitesse des bulles, de longueur de corde des bulles et d'aire interfaciale. En outre, une information statistique sur les mouvements turbulents des bulles est présentée. Chacun des doubles capteurs est. testé. avec la mesure globale de vide en utilisant une pression différentielle. Le résultat est très satisfaisant. La fraction de vide moyennée selon l'airc et la concentration d'aire interfaciale obtenues par les mesures avec les capteurs doubles se comparent bien avec les mesures photographiques. Les résultats montrent que la méthode est précise et convient pour les mesures locales d'aire interfaciale et de fraction de vide dans les écoulements diphasiques à bulles. On présente des résultats pour ces écoulements à différents débits de liquide.

ÖRTLICHE MESSUNG DER GRENZFLÄCHE IN EINER BLASENSTRÖMUNG

Zusammenfassung—Die theoretische Grundlage des Verfahrens zur Messung der zeitlich gemittelten örtlichen Grenzfläche durch Verwendung einer Doppelsonde wird vorgestellt. Meßergebnisse werden für die radiale Verteilung des volumetrischen Dampfgehaltes, der Blasengeschwindigkeit, der Blasengröße und der Konzentration der Grenzfläche bei unterschiedlichen Gasstromdichten mitgeteilt. Außerdem werden einige statistische Informationen über turbulente Bewegungen der Blasen gegeben. Jede der Doppelsonden wird gegen die globale Dampfgehaltsmessung mittels Differenzdruck überprüft. Die Ergebnisse sind sehr zufriedenstellend. Ferner zeigt der Vergleich des flächengemittelten Dampfgehaltes und der Grenzflächenkonzentration—einerseits aus der Messung mit den Doppelsonden, andererseits aus fotografischen Messungen—eine sehr gute Übereinstimmung. Die Doppelsondenmethode erweist sich als präzise und zuverlässig für örtliche Messungen der Grenzfläche und des volumetrischen Dampfgehaltes in einer zweiphasigen Blasenströmung. Abschließend werden einige Meßergebnisse für Blasenströmung bei unterschiedlichen Massenstromdichten der Flüssigkeit dargestellt.

ЛОКАЛЬНОЕ ИЗМЕРЕНИЕ ПЛОЩАДИ ГРАНИЦЫ РАЗДЕЛА ПРИ ПУЗЫРЬКОВОМ ТЕЧЕНИИ

Аннотация—Описывается теоретическое обоснование метода измерения осредненной по времени локальной площади границы раздела с использованием сдвоенного датчика. Приводятся экспериментальные данные по радиальным профилям объемного паросодержания, скорости движения пузырьков, длине пузырьковой цепочки и концентрации межфазной площади при различных значениях расхода газа. Приводятся также некоторые статистические данные о турбулентном движении пузырьков. Получено удовлетворительное согласие результатов измерений с помощью сдвоенных датчиков и данных, основанных на определении дифференциального давления. Кроме того, результаты осредненного по площади объемного паросодержания и концентрации межфазной площади, полученные при эзмерении сдвоенным датчиком, очень хорошо согласуются с данными фотографических измерений. Показано, что использование сдвоенного датчика дает точные и надежные результаты при локальном измерении площади поверхности раздела и объемного паросодержания при пузырьковом двухфазном течении. Представлены некоторые данные измерений концентрации межфазной площади с помощью такого датчика в случае пузырькового течения при различных значениях расхода жидкости.